Available online at www.sciencedirect.com
ScienceDirect
Nuclear Physics B 908 (2016) 151–160
NUCLEAR PHYSICS B
www.elsevier.com/locate/nuclphysb

First neutrino oscillation measurements in NOvA

M.D. Messier [1]

Indiana University, Bloomington, IN 47405, USA

Received 23 February 2016; received in revised form 15 April 2016; accepted 15 April 2016

Available online 20 April 2016

Editor: Tommy Ohlsson

Abstract

The NOvA experiment uses the Fermilab NuMI neutrino beam and a newly constructed 14 kt detector to address several open questions in neutrino oscillations including the neutrino mass hierarchy, the precise value of the angle θ_{23}, and the CP-violating phase $\delta_{\rm CP}$. The experiment has been running since 2014 and has recently released its first results from an equivalent exposure of 2.74×10^{20} protons-on-target equal to 8% of the eventual data set. Measurements of $\nu_\mu \to \nu_\mu$ oscillations find $\Delta m^2_{32} = (2.52^{+0.20}_{-0.18}) \times 10^{-3}$ eV^2 and $0.38 < \sin^2\theta_{23} < 0.65$ for the normal neutrino mass hierarchy. The experiment has observed $\nu_\mu \to \nu_e$ oscillations at 3.3 σ C.L. in this early data and disfavors the inverted neutrino mass hierarchy in the range $0.1\pi < \delta_{\rm CP} < 0.5\pi$ at the 90% C.L.

1. Introduction

Following the discovery of neutrino oscillations [1,2], and hence neutrino mass, many experiments have used neutrinos from the atmosphere [3–5], the Sun [6–10], reactors [11–14], and accelerators [4,15–20] to test the oscillation model and elucidate the parameters of the oscillations. From this program, we now know that two neutrinos are relatively close in mass, separated by $\Delta m^2_{21} = +7.5 \times 10^{-5}$ eV^2 and a third is separated from these by a larger splitting $|\Delta m^2_{32}| = 2.4 \times 10^{-3}$ eV^2. We learned that the mixing angle most responsible for atmospheric

E-mail address: messier@indiana.edu.

[1] For the NOvA Collaboration.

http://dx.doi.org/10.1016/j.nuclphysb.2016.04.027

neutrino oscillations is nearly maximal $\theta_{23} = 45°$ and that the angle most responsible for solar neutrino oscillations is also large, but not maximal $\theta_{12} = 33°$. Recently we have learned from reactor experiments and long-baseline experiments that the third angle, θ_{13}, though smaller than the others, is also a relatively large 8°. The focus of the current generation of experiments, which includes NOvA, is on the remaining unknowns: the sign of the mass splitting Δm^2_{32}, the precise value of θ_{23}, and the possibility that neutrino oscillations violate CP symmetry.

2. Neutrino oscillations in NOvA

The NOvA experiment uses the fact that the remaining questions in neutrino oscillations can be accessed through the study of $\nu_\mu \to \nu_e$ and $\bar{\nu}_\mu \to \bar{\nu}_e$ oscillations in matter at long baseline. Following [21], these probabilities can be written in a very good approximation as

$$P(\nu_\mu \to \nu_e) = P_{\text{atm}} + 2\sqrt{P_{\text{atm}} P_{\text{sol}}}(\cos\Delta_{32}\cos\delta_{\text{CP}} \mp \sin\Delta_{32}\sin\delta_{\text{CP}}) + P_{\text{sol}} \tag{1}$$

where here and elsewhere the top choice of sign is made for neutrinos and the bottom choice is made for antineutrinos. The direct oscillation probabilities associated with the atmospheric and solar mass-splittings are

$$\begin{aligned}\sqrt{P_{\text{atm}}} &= \sin\theta_{23}\sin 2\theta_{13}\frac{\sin(\Delta_{31} - aL)}{\Delta_{31} - aL}\Delta_{31},\\ \sqrt{P_{\text{sol}}} &= \cos\theta_{23}\sin 2\theta_{12}\frac{\sin(aL)}{aL}\Delta_{21}\end{aligned} \tag{2}$$

where the strength of the matter effect for electron number density N_{e} is parameterized by $a = \pm G_{\text{F}} N_{\text{e}}/\sqrt{2} \simeq 1/3500$ km in the Earth's crust. For NOvA $L = 810$ km, and $E \simeq 2$ GeV giving

$$\begin{aligned}\Delta_{32} \simeq \Delta_{31} &= \frac{1.27\Delta m^2_{32} L}{E} \simeq 1.1\\ \Delta_{21} &= \frac{1.27\Delta m^2_{21} L}{E} \simeq 0.04,\end{aligned} \tag{3}$$

for mass-squared splitting in units of eV^2.

Fig. 1 illustrates how measurements of both $P(\nu_\mu \to \nu_e)$ and $P(\bar{\nu}_\mu \to \bar{\nu}_e)$ by NOvA can resolve the θ_{23} octant, the neutrino mass hierarchy, and the value of δ_{CP}. P_{atm} sets the overall scale of the oscillation probabilities and depends on the combination $\sin^2\theta_{23}\sin^2 2\theta_{13}$. The value of $\sin^2(2\theta_{13})$ is now well known from reactor experiments [11–13], however, the value of $\sin^2\theta_{23}$ can vary between 0.4 and 0.6 as θ_{23} ranges through its current experimentally allowed values [22] in the lower octant, through maximal mixing ($\sin^2\theta_{23} = 0.5$), into the upper octant. The mass hierarchy is accessible through the term $\Delta_{31} - aL$ which beats the unknown sign of Δ_{31} against the known sign of aL. Interference between oscillations at the atmospheric scale and solar scale introduces a dependence on δ_{CP}.

3. The NOvA experiment

NOvA is the second long-baseline experiment to use the NuMI neutrino beam at Fermilab [23]. To enhance the size of the matter effect, and hence sensitivity to the mass hierarchy, the NOvA detector is located as far from the point of neutrino production as practically possible, $L =$ 810 km, at a site along the Ash River Trail in Minnesota. The NOvA beam line was deliberately

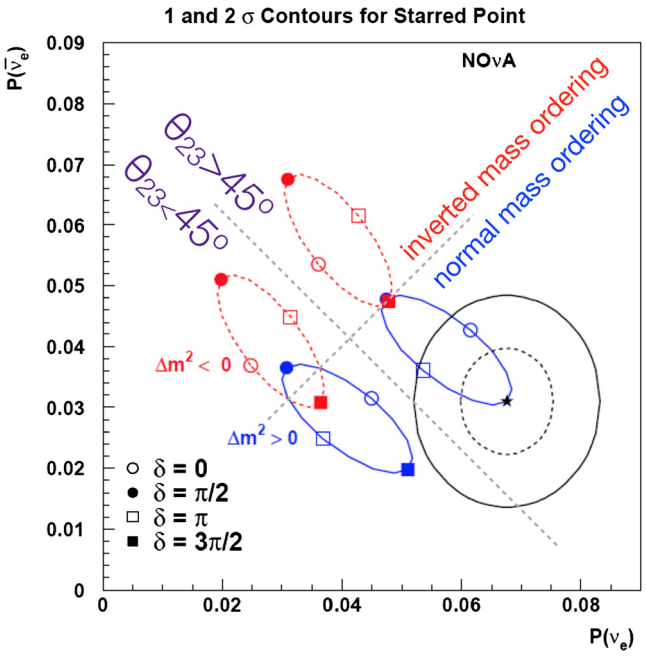

Fig. 1. The oscillation probabilities $P(\nu_\mu \to \nu_e)$ and $P(\bar{\nu}_\mu \to \bar{\nu}_e)$ for the NOvA experiment illustrating the dependence on the remaining unknowns; $\sin^2\theta_{23}$, δ_{CP}, and choice of neutrino mass hierarchy. A possible NOvA measurement is overlaid to demonstrate how NOvA's data might elucidate these remaining unknowns.

chosen to make an angle of 14.6 mrad with respect to the central beam axis to concentrate the neutrino flux near the oscillation maximum and to reduce backgrounds caused by feed down of high energy neutral-current (NC) interactions and by production of $\nu_e + \bar{\nu}_e$ from three-body decays. The resulting spectrum peaks at 2 GeV, has a width of 30%, and in the peak is 97.6% pure ν_μ; $\bar{\nu}_\mu$ contribute 1.7% and $\nu_e + \bar{\nu}_e$ contribute 0.7% to the unoscillated event rates.

The NOvA detector design [24] builds on the concept first outlined in [25] and uses modules made from a custom, highly reflective, blend of polyvinyl chloride (PVC) [27] which contains a large mass of liquid scintillator [26] in 3.9 cm × 6.6 cm × 15.5 m unit cells. A looped 0.7 mm wavelength shifting fiber runs the full length of each cell with both ends terminating on a single pixel of an avalanche photodiode (APD). The APDs have high quantum efficiency, $\simeq 80\%$, which is crucial for seeing the long-wavelength light which is most efficiently transmitted from the far end of a cell. This design yields roughly 29 photoelectrons per cell for a normally incident muon track passing at a distance of 15 m from the readout giving a per-cell detection efficiency of better than 90%.

The detector has a total 9 kt of liquid scintillator contained in a 5 kt plastic structure, 15.5 m high, 15.5 m wide, and 60 m long segmented into 344,000 channels which provide x and y readout in alternating planes. The detector meets the goals of achieving a large detector mass using low Z materials which are optimum for resolving the details of electromagnetic shower shapes, while also achieving a high degree of segmentation which improves neutrino event reconstruction and allows the detector to operate on the surface where the cosmic-ray rate is 140 kHz. Construction of the detector began in July 2012 and was completed in November 2014. Fig. 2 highlights two steps from the assembly of the far detector.

Fig. 2. Left: A student trims excess wave-length shifting fiber from the end of a 32-cell NOvA module at the factory at the University of Minnesota. Right: A single block of the NOvA detector is moved into place at the FD laboratory. *Photo credits: Reidar Hahn, Fermilab.*

A near detector (ND) was assembled underground at the Fermilab site at a distance of 1 km from the neutrino source to characterize the neutrino event spectrum and backgrounds to the electron appearance search at the far detector (FD) prior to oscillations. The ND is smaller (193 t) and is outfitted with a steel muon range stack, but is otherwise identical in construction to the FD.

The NOvA project also undertook a series of improvements to the accelerators at Fermilab to double the power of the NuMI beam. By reducing the cycle time from 2.2 s to 1.3 s and by converting the Recycler Ring to a proton accumulator, the Main Injector is now delivering 500 kW to the NuMI target and regular operation at 700 kW is planned for next year.

Neutrino measurements with the experiment began when the first four of the eventual 14 kt were operational. An initial exposure of 2.74×10^{20} 14-kt equivalent protons-on-target recorded between February 6, 2014 and May 15, 2015 provided first results for $\nu_\mu \to \nu_\mu$ and $\nu_\mu \to \nu_e$ oscillations [19,20]. This initial data set is 8% of the total planned NOvA exposure.

4. Muon neutrino disappearance

As NOvA operates very close to the first oscillation maximum, the ν_μ charged-current (CC) energy spectrum is significantly depleted at the FD and hence quite sensitive to relatively small changes in the oscillation parameters $\sin^2\theta_{23}$ and $|\Delta m^2_{32}|$.

Fig. 3 shows an event display of a ν_μ-CC event candidate recorded in the NOvA FD. The ν_μ-CC analysis proceeds by grouping the calibrated cell hits recorded in coincidence with the neutrino beam arrival according to their proximity to each other in space and time. A Kalman filter-based algorithm searches these hit clusters for tracks resulting from charged-particles and fits the trajectories.

Each of the tracks is evaluated against the muon hypothesis using information on the track multiple scattering angles, the dE/dx profile, the overlap with the hadron recoil, and the length of the track. Fig. 4 shows the distributions of this muon-identification variable for data and simulation in the ND. If the most muon-like track in the event exceeds a threshold of 0.75, the event

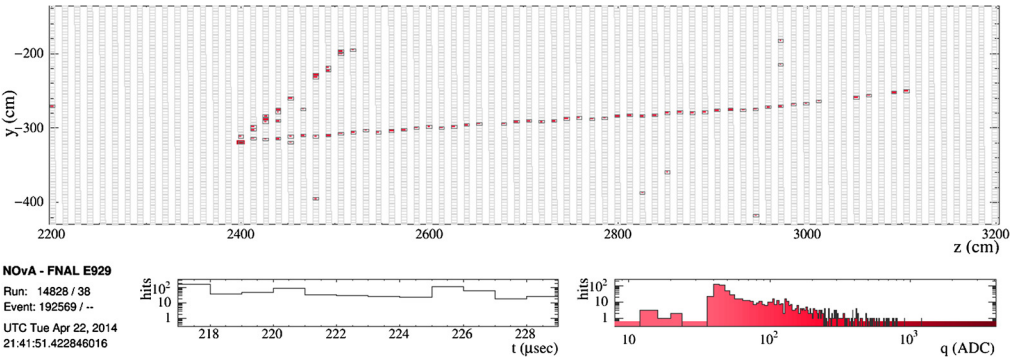

Fig. 3. A ν_μ-CC candidate event recorded in the NOvA far detector. The display is zoomed to the region where the event occurred inside the detector.

is accepted as a ν_μ-CC candidate. Event activity not associated with the tagged muon-track is assumed to be associated with the recoil hadron system.

To ensure a reliable neutrino energy reconstruction and to reject backgrounds from entering particles, events in the ND and FD are required to be contained in the detector active volume by vetoing events with activity in the outer two layers of the detector volume and by requiring several layers of active detector upstream and downstream of the muon track. At the FD, these containment requirements reduce the cosmic-ray backgrounds by roughly a factor of 200. An additional factor of 1000 is achieved using a multi-variate evaluation of the event multiplicity, the event direction and topology, location, track energy deposition.

These selection criteria were optimized using GENIE [28] simulations of signal ν_μ-CC events, NC background events, and real cosmic-ray events recorded outside the neutrino beam spill time window. The selections are 57% efficient at retaining true ν_μ-CC events below 5 GeV. After all selections, cosmic-ray backgrounds are rejected at a rate of 12 million : 1 and are estimated to comprise 4.1% of the sample of events selected for analysis at the FD. Likewise, NC events are reduced at a rate of 100:1 and comprise 6% of the events selected for analysis at the FD. These requirements select a 98% pure sample of 500,000 ν_μ-CC events at the ND which is used to predict the unoscillated ν_μ-CC event spectrum at the FD.

The measured muon track length provides an estimate of the muon energy E_μ with 4% precision. The remaining off-track event energy is summed and converted to a hadronic energy E_{had} using calibration constants derived from simulated events based on the GENIE [28] and GEANT4 [29] packages. Fig. 4 compares the track-length and E_{had} distributions for data and simulation of neutrino events in the ND. The muon track length distributions agree well, but the means of the E_{had} distributions differ by 14%, presumably due to inaccuracies in the modeling of neutrino-nucleus cross-sections. To accommodate this difference, the E_{had} calibration scale is set 14% higher in the data than it is in the simulation which brings the peak locations of the energy spectra in data and simulation into agreement. The neutrino energy is computed as the sum

$$E_\nu = E_\mu + E_{\text{had}} \tag{4}$$

with 7% resolution. Fig. 4 shows comparisons of the muon track length distributions, the E_{had} distributions, and the E_ν distributions for data and simulation in the ND.

When applied at the FD, 33 events are observed below 5 GeV of which 3.4 are expected to be backgrounds from cosmic-ray and NC events. Before oscillations this spectrum is expected

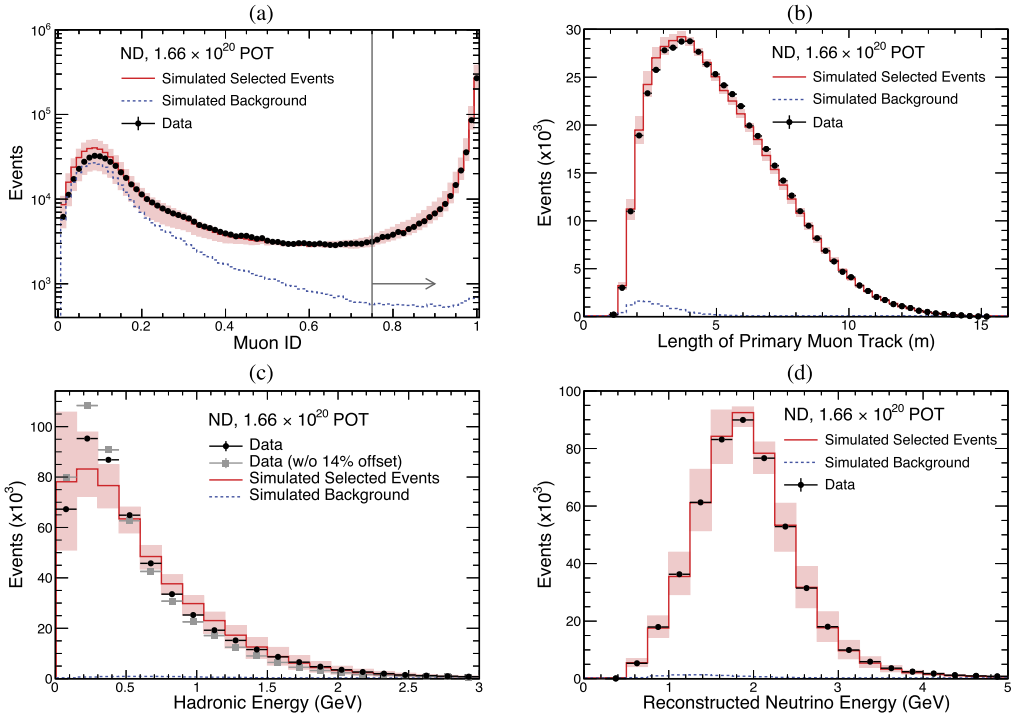

Fig. 4. Comparisons of data and simulation for ν_μ-CC candidate events identified in the NOvA near detector. Top left: The muon-track particle identification parameter. Top right: Muon track-length. Bottom left: Hadronic energy distributions, shown w/o the 14% calibration applied and with the 14% calibration applied. Bottom right: the total reconstructed neutrino energy.

to contain 211.8 ± 12.5 (syst.) based on extrapolations from the ND measurements. The energy spectrum of the events is shown in Fig. 5 with comparisons to the un-oscillated prediction and best-fits for oscillations.

The event counts in 18 bins ranging from 0.5 GeV to 5.0 GeV are fit using a maximum likelihood estimator by varying $\sin^2\theta_{23}$ and Δm^2_{32} in a three-flavor oscillation model. In the fit, the parameters Δm^2_{21}, θ_{12}, and θ_{13} vary within the ranges allowed by current experiments. The phase δ_{CP} is left unconstrained. During the fit, the effects of all important sources of systematic uncertainty are accounted for of which the most important is the uncertainty in the absolute energy scale, much of which results from uncertainties in the hadronic energy distribution. We measure $\Delta m^2_{32} = (2.52^{+0.20}_{-0.18}) \times 10^{-3}$ eV^2 and $0.38 < \sin^2\theta_{23} < 0.65$ at 68% C.L. The mixing angle has two degenerate best-fit points at $\sin^2\theta_{23} = 0.43$ and 0.60. Currently, $\sin^2\theta_{23}$ has a 6.8% systematic uncertainty, of which 4.1% results from uncertainty in the absolute energy scale; Δm^2_{32} has a 3.7% systematic uncertainty of which 2.6% results from the absolute energy scale.

5. Electron neutrino appearance

An example ν_e-CC event in the NOvA FD is shown in Fig. 6. The process of selecting these events initially proceeds in the same way as the selection of ν_μ-CC events; the signals recorded in the detector coincident with the arrival of the neutrino pulse from the Fermilab are clustered

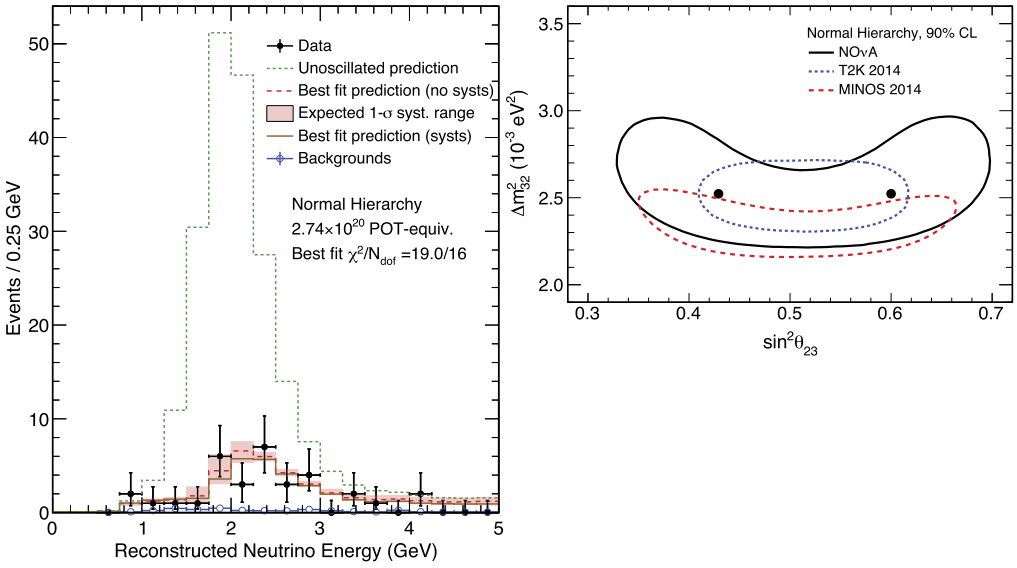

Fig. 5. Top: The predicted unoscillated ν_μ-CC spectrum at the FD compared to data and best-fit expectations including oscillations. Bottom: The values of Δm^2_{32} and $\sin^2\theta_{23}$ allowed at 90% C.L. allowed by a fit to the FD energy spectrum.

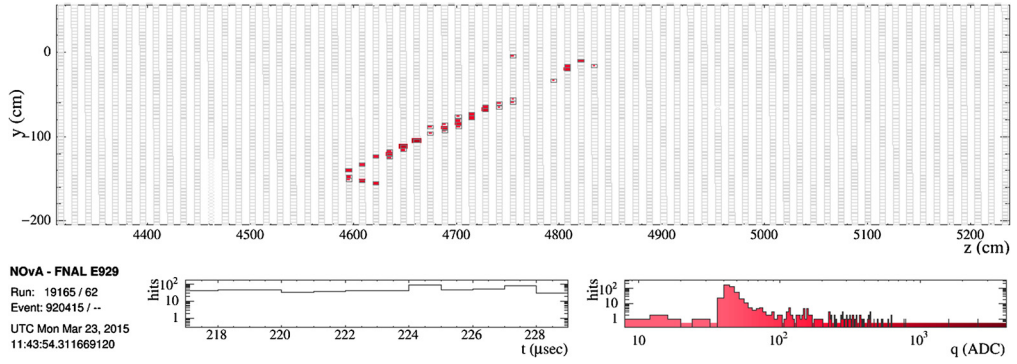

Fig. 6. A candidate ν_e-CC event recorded by the NOvA far detector. The display is zoomed to the region where the event occurred inside the detector.

based on their time and spatial correlations. These clusters are further analyzed to identify the event vertex and organize the hits into particle tracks [30]. Events with energies in the oscillation signal region between 1.3 and 2.7 GeV which lack a clear muon track are selected for further analysis.

Electromagnetic shower development depends on the Moliere radius in the transverse direction and on the radiation length in the longitudinal direction. These correspond to $\simeq 3$ cell-widths and $\simeq 6$ planes in NOvA. We test candidate events against this expected shower topology to further improve the ν_e-CC purity of the selected sample using two techniques. The first technique, "LID", is based on a likelihood comparison of the leading shower to templates calculated for various particle hypotheses including electrons, photons, protons, and pions. These likelihoods are used as inputs to an artificial neutral net which is tuned to select ν_e-CC events and

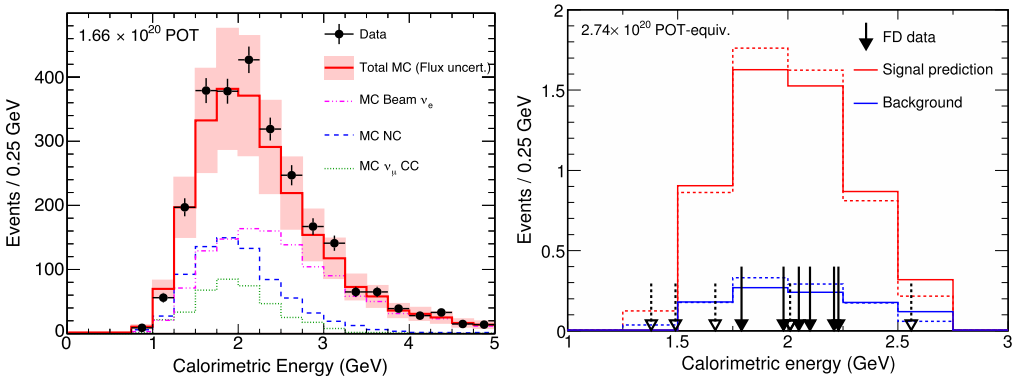

Fig. 7. Left: The distributions of calorimetric energy for ν_e-CC candidate events reconstructed in the ND for both data and Monte Carlo (MC) simulations. Right: The expected signal and background energy distributions for ν_e-CC candidate events using the LID (solid) and LEM (dashed) selectors. Arrows indicate the locations of the 6 events identified by both LID and LEM (solid) and the 5 events identified only by LEM (dashed). (For interpretation of the references to color in this figure legend, the reader is referred to the web version of this article.)

reject background events from ν_μ-CC events, NC events, and events from cosmic-rays. A second method, "LEM", attempts to match the entire event topology to a large library of simulated signal and background events searching for the best matches [31]. These two rather different approaches achieve signal efficiencies of 34% and 35% respectively and agree on the signal event classification in 62% of the events; both reject 99% of neutrino backgrounds and achieve better than $1:10^8$ rejection against cosmic-ray backgrounds. Prior to examining the FD data, LID was chosen for the primary analysis.

Fig. 7 shows the energy spectra of the events selected by the LID algorithm in the ND and FD. The event rate is 7% greater in the ND data than calculated from simulations. These spectra are extrapolated to the FD and predict 0.93 events of background from beam sources. Data recorded outside the beam-on time window predicts 0.06 background events from cosmic-rays. The total background prediction is 10.8% uncertain primarily due to uncertainties related to the composition of the background samples, calibration, and the performance of the liquid scintillator near saturation.

The FD recorded 6 events which pass the LID selection and 11 events satisfying LEM. These are 3.3 σ and 5.3 σ excesses over background. All 6 of the LID events are contained in the LEM sample. This distribution of event counts, or one less likely, is expected to occur by chance in 7.8% of cases.

The observed event counts are compared to expectations based on oscillations to extract information on the neutrino mass hierarchy and δ_{CP}. In the comparisons, the ν_e-CC signal efficiency is varied by $\pm 17.6\%$ to account for systematic uncertainties largely arising from uncertainties in the neutrino-nucleus interaction model. Fig. 8 shows the confidence intervals [32] for the oscillation parameters $\sin^2 2\theta_{13}$ and δ_{CP} computed for the case $\sin^2\theta_{23} = 0.5$; all other oscillation parameters are varied within their experimental limits. Our observations and measurements of θ_{13} from reactors show the best agreement when the normal hierarchy is chosen with $\pi < \delta_{CP} < 2\pi$.

Fig. 8 uses the reactor constraint $\sin^2 2\theta_{13} = 0.086 \pm 0.005$ to compute the likelihood ratios for different choices of the neutrino mass hierarchy and δ_{CP}. The range from $0.1\pi < \delta_{CP} < 0.5\pi$ in the inverted hierarchy case is disfavored at 90% confidence level. The results for LEM, which selected more events, exclude the inverted hierarchy at $> 2\ \sigma$ at the expense of a trial factor for

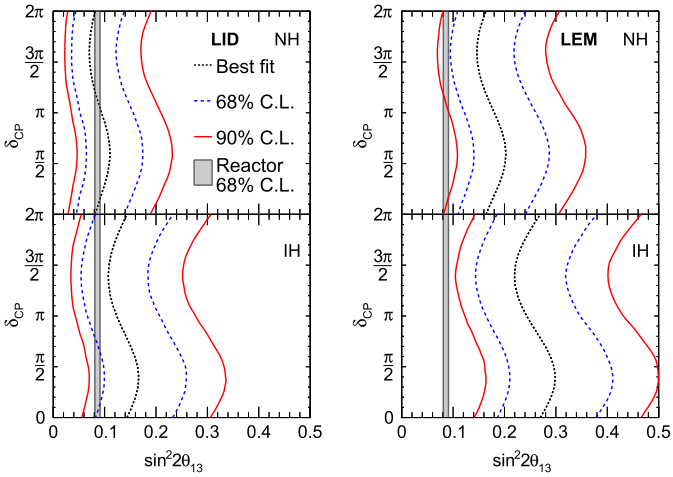

Fig. 8. Allowed values of δ_{CP} vs. $\sin^2 2\theta_{13}$. The normal hierarchy (NH) cases are shown in the top panels while the inverted (IH) case is shown in the bottom panels. Panels on the left use the primary LID event selector while those on the right using the secondary LEM selector.

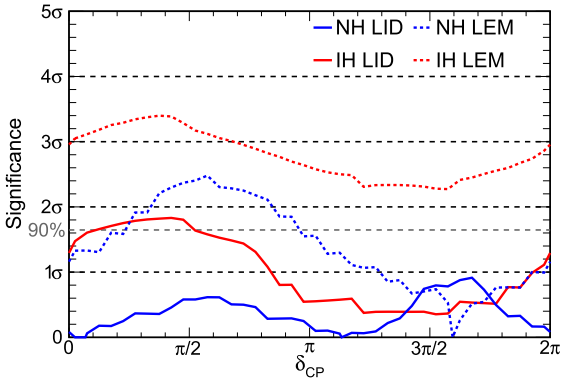

Fig. 9. Significance of the difference between the measured and predicted event counts as a function of δ_{CP} and choice of neutrino mass hierarchy (NH and IH). The solid curves use the primary LID selector and the dotted curves use the secondary LEM selector. (For interpretation of the references to color in this figure legend, the reader is referred to the web version of this article.)

having analyzed the same data sample in two ways (see Fig. 9). We expect to double the size of our data set by summer of 2016 which should help clarify the interesting possibilities raised by this early data and we will collect a factor 10 more data before the end of the experiment run.

Acknowledgements

This work was supported by the US Department of Energy; the US National Science Foundation; the Department of Science and Technology, India; the European Research Council; the MSMT CR, Czech Republic; the RAS, RMES, and RFBR, Russia; CN Pq and FAPEG, Brazil; and the State and University of Minnesota. We are grateful for the contributions of the staffs of the University of Minnesota module assembly facility and NOvA FD Laboratory, Argonne

National Laboratory, and Fermilab. Fermilab is operated by Fermi Research Alliance, LLC under Contract No. De-AC02-07CH11359 with the US DOE.

References

[1] Y. Fukuda, et al., Super-Kamiokande Collaboration, Phys. Rev. Lett. 81 (1998) 1562.
[2] Q.R. Ahmad, et al., SNO Collaboration, Phys. Rev. Lett. 89 (2002) 011301.
[3] R. Wendell, et al., Super-Kamiokande Collaboration, Phys. Rev. D 81 (2010) 092004.
[4] P. Adamson, et al., MINOS Collaboration, Phys. Rev. Lett. 112 (2014) 191801.
[5] M.G. Aartsen, et al., IceCube Collaboration, Phys. Rev. Lett. 111 (8) (2013) 081801.
[6] B.T. Cleveland, T. Daily, R. Davis Jr., J.R. Distel, K. Lande, C.K. Lee, P.S. Wildenhain, J. Ullman, Astrophys. J. 496 (1998) 505.
[7] J.N. Abdurashitov, et al., SAGE Collaboration, Phys. Rev. C 80 (2009) 015807.
[8] K. Abe, et al., Super-Kamiokande Collaboration, Phys. Rev. D 83 (2011) 052010.
[9] B. Aharmim, et al., SNO Collaboration, Phys. Rev. C 88 (2013) 025501.
[10] G. Bellini, et al., Phys. Rev. Lett. 107 (2011) 141302.
[11] T. Abrahão, et al., Double Chooz Collaboration, J. High Energy Phys. 1601 (2016) 163.
[12] J.H. Choi, et al., RENO Collaboration, arXiv:1511.05849 [hep-ex].
[13] F.P. An, et al., Daya Bay Collaboration, Phys. Rev. Lett. 115 (11) (2015) 111802.
[14] A. Gando, et al., KamLAND Collaboration, Phys. Rev. D 88 (3) (2013) 033001.
[15] M.H. Ahn, et al., K2K Collaboration, Phys. Rev. D 74 (2006) 072003.
[16] P. Adamson, et al., MINOS Collaboration, Phys. Rev. Lett. 110 (17) (2013) 171801.
[17] N. Agafonova, et al., OPERA Collaboration, PTEP 2014 (10) (2014) 101C01.
[18] K. Abe, et al., T2K Collaboration, Phys. Rev. D 91 (7) (2015) 072010.
[19] P. Adamson, et al., NOvA Collaboration, Phys. Rev. Lett. 116 (2016) 151806.
[20] P. Adamson, et al., NOvA Collaboration, Phys. Rev. D 93 (5) (2016) 051104.
[21] H. Nunokawa, S.J. Parke, J.W.F. Valle, Prog. Part. Nucl. Phys. 60 (2008) 338.
[22] K.A. Olive, et al., Particle Data Group Collaboration, Chin. Phys. C 38 (2014) 090001.
[23] P. Adamson, et al., Nucl. Instrum. Methods A 806 (2016) 279.
[24] D.S. Ayres, et al., NOvA Collaboration, FERMILAB-DESIGN-2007-01.
[25] P. Border, et al., Nucl. Instrum. Methods A 463 (2001) 194.
[26] S. Mufson, et al., Nucl. Instrum. Methods A 799 (2015) 1.
[27] R.L. Talaga, J.J. Grudzinski, S. Phan-Budd, A. Pla-Dalmau, J.E. Fagan, C. Grozis, K.M. Kephart, arXiv:1601.00908 [physics.ins-det].
[28] C. Andreopoulos, et al., Nucl. Instrum. Methods A 614 (2010) 87.
[29] S. Agostinelli, et al., GEANT4 Collaboration, Nucl. Instrum. Methods A 506 (2003) 250.
[30] M. Baird, J. Bian, M. Messier, E. Niner, D. Rocco, K. Sachdev, J. Phys. Conf. Ser. 664 (7) (2015) 072035.
[31] C. Backhouse, R.B. Patterson, Nucl. Instrum. Methods A 778 (2015) 31.
[32] G.J. Feldman, R.D. Cousins, Phys. Rev. D 57 (1998) 3873.

Further reading

[33] Y. Abe, et al., Double Chooz Collaboration, J. High Energy Phys. 1410 (2014) 086.